A Study of Pore Blockage in Silicalite Zeolite Using Free Energy Perturbation Calculations

Amit Gupta and Randall Q. Snurr*

Department of Chemical and Biological Engineering and Center for Catalysis and Surface Science, Northwestern University, Evanston, Illinois 60208

Received: June 16, 2004; In Final Form: October 16, 2004

Binary systems consisting of large coadsorbed molecules (*n*-hexane, cyclohexane, and benzene) with smaller penetrant molecules (methane) were simulated to investigate the mechanisms of pore blockage in the zeolite silicalite. Benzene and cyclohexane trap the methane molecules in the zeolite channels on the time scales of molecular dynamics simulations. Minimum energy paths for methane diffusion past the blocking molecules were determined, and free energy perturbation calculations were carried out along the paths to get the rate constants of methane hopping past coadsorbed benzene and cyclohexane molecules, which adsorb in the channel intersections. Three principal diffusion pathways were found in both the methane/benzene and methane/cyclohexane systems. Minima which were connected by low-energy pathways were grouped together into macrostates. Using the calculated hopping rates between macrostates, kinetic Monte Carlo was then used to obtain the diffusivity of methane with a coadsorbate benzene loading such that all channel intersections are filled by benzene — conditions where molecular dynamics simulations fail. Passage of methane across cyclohexane molecules involved pushing the cyclohexane molecules into the channels from their preferred channel intersection positions.

Introduction

Molecular dynamics (MD) simulation is a very useful technique for the study of equilibrium and transport properties of materials due to its ability to track the physical motion of molecules with no assumptions beyond those of the molecular models employed. MD has been particularly useful in the study of crystal lattice dynamics and diffusion in zeolites. The diffusion of small molecules within zeolite pores can play a major role in adsorption separations and catalytic processes using zeolites as well as in zeolite membranes currently under development. MD simulations of diffusion in zeolites began with simple molecules such as methane and xenon and progressed to more complex molecules such as benzene and longer *n*-alkanes. These studies have been reviewed by several authors.[1−4] In parallel with the evolution from simple molecules to more complex sorbates, the simulations have moved from equilibrium MD calculations of the self-diffusion coefficient to calculation of the Fickian, Onsager, or Maxwell−Stefan diffusivities using either equilibrium MD[5] or various nonequilibrium methods.[6]

Encouraged by the success of single-component simulations, in recent years there has been an increasing effort to extend the techniques to multicomponent systems. For example, Snurr and Kärger[7] performed MD simulations for mixtures of methane and CF_4 in silicalite to compare against self-diffusivity data obtained from pulsed field gradient (PFG) NMR experiments. They found generally good agreement between simulation and experiment. Gergidis and Theodorou[8] used MD simulations to examine the dynamics of methane and *n*-butane coadsorbed in silicalite. They investigated the effects of methane and *n*-butane loading on the self-diffusivity and siting of both components. They also studied the effects of loading on the *n*-butane conformation and observed a region of "anomalous diffusion" where the mean-square displacements do not scale linearly with time. More recently, Sanborn and Snurr[9] did a similar analysis of binary mixtures of CF_4 with a number of *n*-alkanes in faujasite. They examined the effects of both loading and carbon number on the diffusivities and siting of the components. Diffusivity trends were explained using free volume arguments and single-component molecular mobilities. In addition, they calculated Fickian transport diffusivities of methane/CF_4 mixtures from their equilibrium MD simulations.[9,10] Subsequently, Kamala et al.[11] used equilibrium MD to calculate Fickian diffusivities for Ar/Kr mixtures in NaY, and Skoulidas et al.[12] studied methane/CF_4 mixtures in silicalite.

In this paper we are interested in the effects of coadsorbing larger molecules on the dynamics of smaller penetrant molecules, in an effort to gain insight into the mechanisms of pore blockage in zeolites. Investigation of zeolite deactivation by simulation remains a relatively unexplored area. Theodorou and Wei[13] first studied pore blockage using a lattice model simulation. Förste et al.[14] studied the same phenomenon using PFG NMR and lattice simulations of a methane/benzene system in silicalite. Förste et al. obtained very different diffusion profiles from their lattice model simulations for methane, depending on whether the benzene was located in the intersections or the channels. These results led them to conclude that benzene adsorbs preferentially in the intersections. These coarse-grained lattice models used the rates of "passing" the blockage as empirical parameters for the simulations. Similarly, Nelson et al.[15] used a simple lattice model to simulate the formation of coke in ZSM-5 during the conversion of methanol to gasoline. They used a number of empirical parameters to study the distribution of coke within the zeolite as a function of reactant pressure. Other lattice model studies are reviewed by Keil et al.[4] The objective of this work is to understand the mechanisms of pore blockage at a more molecular level and hence obtain

* To whom correspondence should be addressed: Fax 1-847-467-1018, Tel 1-847-467-2977, e-mail snurr@northwestern.edu.

10.1021/jp047391e CCC: $30.25
Published on Web 01/13/2005

diffusivities and rate constants in a fully predictive manner which can be compared against experimental data.

We use benzene, cyclohexane, and *n*-hexane as representative larger molecules that can block the diffusion of smaller methane penetrants. We examine the effects of the loading of the coadsorbed "blockage" molecules on the dynamics of methane. In addition, we report the effects of the channel geometry on the dynamics of the penetrants. By comparing the results of the benzene, cyclohexane, and *n*-hexane systems, we expect to get some insight into the effect of the nature of the pore blockage on the molecular level dynamics.

In this paper a number of different simulation techniques are employed. We describe in turn each technique and its implementation, followed by the results produced with that technique. First, the potential model used to describe the molecular interactions in all of the calculations is presented. We then discuss molecular dynamics simulations and the results of coadsorbate loading on the diffusivity of methane. This leads into a description of the need for rare event simulations and methodologies to study methane hopping past the blockages. We present minimum energy paths and use thermodynamic perturbation calculations to get the free energy of activation for the passage of methane across the blocking molecules. Since MD works reasonably well for up to three molecules of cyclohexane or benzene per unit cell, we focus on simulating the passage of methane at a coadsorbate loading of four molecules per unit cell. At this loading all four intersections in a silicalite unit cell are occupied, and initially we hypothesize that the blocking molecule does not leave the intersection on the time scales of methane passage. Later in the paper we examine the validity of this hypothesis. This assumption is used in a kinetic Monte Carlo simulation to fix the positions of the blocking molecule in the intersections and obtain the diffusivity of methane.

Molecular and Potential Model

All simulations were done in silicalite, which is the siliceous form of the commercially important zeolite ZSM-5. Silicalite exists in three crystalline forms described by van Koningsveld et al.[16] We used the ORTHO form of silicalite for our work. The pore structure consists of zigzagging channels running along the *x* direction and intersecting straight channels running along the *y* direction. There are no pores in the *z* direction, and any motion in this direction has to be through a tortuous path in the zigzag and straight channels. The channels are roughly 5.5 Å wide, and they meet to form large channel intersections. There are four straight channels, four zigzag channels, and four intersections per unit cell of silicalite. To aid in the discussion, the different sites are marked in Figure 1. The zeolite framework was held rigid. As in the work of Kiselev et al.,[17] the silicon interactions were not explicitly included in the zeolite/sorbate Lennard-Jones interactions. For simulations with adsorbed benzene, partial charges of −1.0 and +2.0 were placed on the oxygen and silicon atoms, respectively, as in the work of Snurr et al.[18]

Methane was modeled as a single Lennard-Jones united atom. The methane/methane and methane/silicalite parameters were taken from Goodbody et al.[19] The methyl and methylene units in *n*-hexane were also treated as neutral united atoms with identical potential Lennard-Jones parameters but different masses. The bond lengths were fixed at 1.53 Å. Fluctuations of the bond angle defined by three adjacent united atoms were described by a harmonic potential. Dihedral rotations about adjacent, nonterminal united atoms were described by a six term

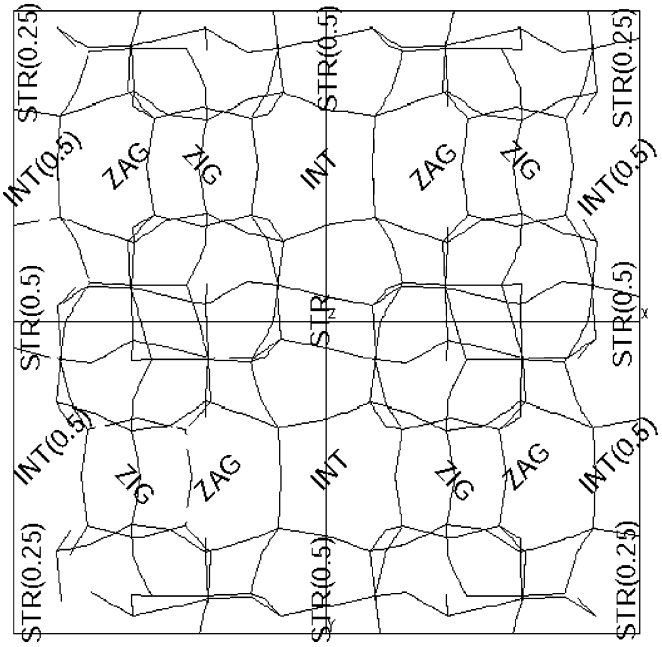

Figure 1. Site definitions in silicalite. There are 4 intersection (INT), 4 zigzag channels (ZIG and ZAG), and 4 straight channels (STR) per unit cell. The fraction of each site shown in the figure, if different from 1, is marked in parentheses. The view shown looks down the *z* axis of the zeolite.

cosine expansion. *n*-Hexane includes an extra intramolecular interaction to prevent the backbone from crossing back onto itself; this is a Lennard-Jones interaction arising between all intramolecular atomic pairs that are separated by more than three atoms. All the potential parameters for *n*-hexane were taken from June et al.[20] Following Rowley and Ely,[21] we used the same force field for cyclohexane as for *n*-hexane, except for the nonbonded, one−four, intramolecular term, which was discarded.

Benzene was modeled as a 12-centered molecule with explicit carbon and hydrogen atoms. The potential parameters for benzene/benzene and benzene/zeolite interactions were described by Lennard-Jones plus Coulombic terms. The parameters were taken from Snurr et al.[18]

The intermolecular binary interaction parameters were obtained using the Lorentz−Berthelot rule as described previously.[22]

Effect of Loading: MD Simulations

Molecular dynamics simulations were done in the microcanonical ensemble (NVE) using Gear's six-value, five-parameter predictor−corrector method. The bond lengths were constrained using the method of Edberg, Evans, and Morris based on Gauss's principle of least constraints.[23] Since the constraint matrix for benzene is singular,[24] we used the algorithm of Ciccotti[25] to implement the constraints. This algorithm was recast in terms of Gauss's principle of least constraints to use the Edberg, Evans, and Morris scheme as described elsewhere.[26] Initial configurations for MD were generated by grand canonical Monte Carlo simulations.[22]

To examine the effect of the loading of the coadsorbed molecule, the loading of methane was kept constant at 3 molecules per unit cell while the loading of the coadsorbed molecules was changed from 0 to 4 molecules per unit cell. The simulations were done at 300 K. A simulation cell size of $2 \times 4 \times 4$ unit cells was used for coadsorbate loadings of 1

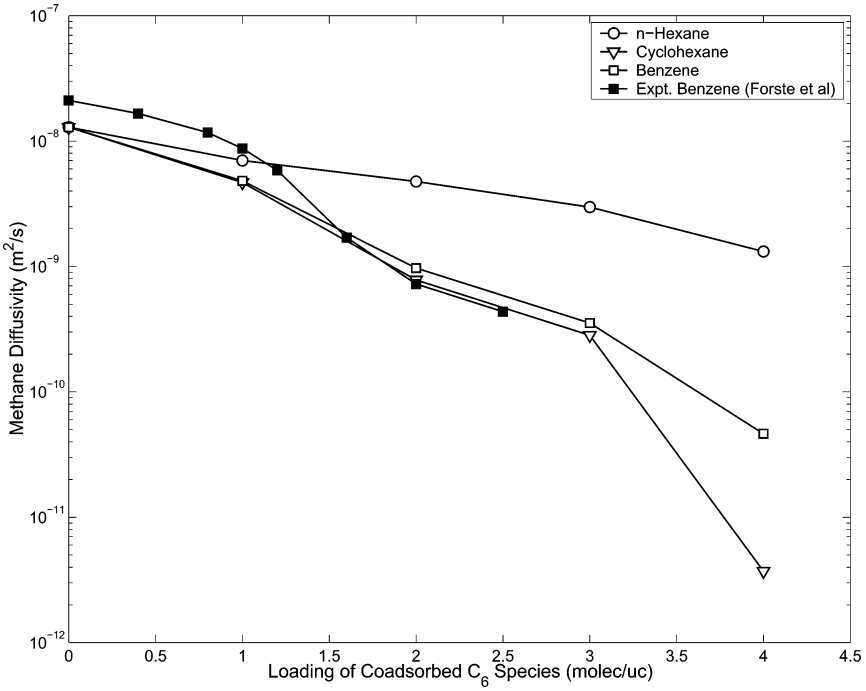

Figure 2. MD simulation of 3 molecules per unit cell of methane with different loadings of coadsorbed molecules.

and 2 molecules per unit cell and $2 \times 2 \times 4$ for coadsorbate loadings of 3 and 4 molecules per unit cell. The system was equilibrated until the atomic and molecular temperatures were equal and within ± 5 K of the set temperature.[24] The equilibration runs were typically 1−2 ns long. Production run lengths were 0.5−2 ns with an integration step size of 1.5−2 fs. The configurations were written to file every few hundred femtoseconds and later analyzed to get the energies and diffusivities. The standard deviation of the total energy over the entire run length was on the order of 0.3%. The self-diffusivities were calculated as orientationally averaged values.

Figure 2 shows the self-diffusivity of methane as a function of the loading of the coadsorbed molecules from MD. The methane diffusivity decreases as the loading of the larger, slower moving coadsorbed molecules is increased, indicating that the methane is being blocked by these bulkier molecules. Since *n*-hexane is the most flexible and mobile, we expect it to have the least blocking effect on the methane. This is confirmed by the fact that the decrease in the diffusivity of methane is much more gradual with *n*-hexane as compared to the other coadsorbates. With coadsorbed benzene or cyclohexane, the methane diffusivity drops by several orders of magnitude. The diverging nature of the diffusivities as the loading is increased is indicative of differences in the blocking characteristics of the three coadsorbates. The filled squares in Figure 1 are the PFG NMR self-diffusivity measurements of Förste et al.[14] The experimental results also exhibit a decrease in self-diffusivity with loading and give good quantitative agreement with methane/benzene simulations.

The adsorption sites of the coadsorbed molecules play a significant role in determining the diffusivity trends. *n*-Hexane preferentially adsorbs in the silicalite channels,[20] where it can affect the penetrant traffic solely through that channel. The other coadsorbates adsorb in the relatively open channel intersections,[22] where they can block the traffic from the four channels that meet at that intersections, thus providing greater pore blockage. At 4 molecules per unit cell, all of the intersections of the unit cell are occupied by benzene or cyclohexane, effectively trapping the methane molecules in the channels on MD time scales. This is evident from the steep decrease in the diffusivity between 3 and 4 molecules per unit cell. Similar behavior was observed by Schuring et al.,[27] who used the tracer-exchange positron emission profiling technique (TEX-PEP) to obtain the adsoption and diffusion constants of *n*-hexane/2-methylpentane mixtures in silicalite. By varying the relative gas phase pressure of *n*-hexane and 2-methylpentane, they studied the siting, adsorption, and diffusion properties of the system as a function of loading. They observed that due to the branched geometry of 2-methylpentane it adsorbed preferentially in the channel intersections, and as the loading of 2-methylpentane was increased from 3 to 4 molecules per unit cell the mobility of *n*-hexane decreased steeply.

From a simulation viewpoint, molecular dynamics is not very efficient at tracking diffusivities lower than about 10^{-10} m^2/s. Hence, the diffusivities of methane at 4 molecules per unit cell in Figure 2 are at best rough estimates. The rest of the paper discusses other approaches for studying the diffusivity of methane in this low diffusivity regime.

Minimum Energy Paths

There are two distinct time scales in the motion of methane at high loadings of coadsorbed benzene or cyclohexane. The rattling motion of methane between two blocking molecules takes place on much faster time scales than the motion of the methane past the blocking molecule. Since the MD integration time step is governed by the faster rattling motion, it is unable to track the passing events. This separation of time scales, however, makes the system amenable to transition-state theory calculations, where one of the assumptions is that transitions take place between equilibrated states of the system.

Fundamental inputs to a transition-state theory calculation are the minimum energy paths. The minimum energy path (MEP) consists of intermediate lowest energy states of a system between two minima or equilibrated states.[28] The highest point along the MEP is a first-order saddle point in the energy hypersurface. The minimum energy paths thus enable one to connect the various minima of a system into physical dynamical

paths in addition to providing the activation energies for transitions between the minima. This information is of central importance in describing translational dynamics and for calculating free energy changes and rates from transition-state theory.

There are a number of methods for getting the minimum energy paths of a system. Often the first step is to find the minima in the potential energy hypersurface. Depending on the ease of evaluation of the gradient of the potential function and the dimensionality of the system, there are a number of techniques for getting the minima.[29] The minimum energy path can then be obtained by three basic methods. One can locate the first-order saddle points and then follow a steepest-descent trajectory from the saddle point to the connecting minima using the intrinsic reaction coordinate approach (IRC) of Fukui.[30] Again depending on the dimensionality of the system, locating the saddle points may or may not be feasible, and Bell and Crighton[31] review a number of techniques for this purpose. The second class of methods can be used where it is difficult to locate the saddle points. In this so-called "dragging" method, the system is taken from one minimum to the next by constraining one degree of freedom and minimizing over the rest.[32] The constrained degree of freedom is then used as a "reaction coordinate". More recently, a third class of methods have emerged in which a "chain" of states of the system is generated at discrete points between the end-point configurations, and all the intermediate images are optimized simultaneously in some concerted way.[28,33,34]

To investigate the mechanism of blockage of methane, we chose as our system two benzene or cyclohexane molecules in adjoining intersections with a single methane molecule in the connecting channel. For simplicity, the cyclohexane molecules were kept rigid in their chair conformation. With this approximation the positions of benzene and cyclohexane molecules can be described using six generalized coordinates (three center-of-mass coordinates and three Eulerian angles). Thus, the overall dimensionality of the system was 15. We compared two different methods for getting the minimum energy paths: the dragging method and the IRC approach starting from the saddle points.[35]

MEP Methods

Details of how we implemented the dragging method are described elsewhere.[26] Two sets of simulations were done for both cyclohexane and benzene, one with the methane between the coadsorbed molecules in the straight channel and one with the methane in the zigzag channel. The methane was initially placed in the middle of the channel. Following the topology of silicalite, the reaction coordinate for the straight channel was along the *y*-axis and for the zigzag channel along the *x*-axis. We found that the dragging method is subject to a great deal of error in its implementation if there are multiple paths along a given channel. With the system constrained at a particular point along the reaction coordinate, searches for local minima are performed, and then the minima in the different planes along the reaction coordinate must be connected to form continuous paths. However, the more or less ad hoc heuristics used to connect the minima can lead to unphysical jumps of the system between two different paths. In addition, some paths can terminate prematurely if the search for minima in each plane does not find the high-lying minima.

As an alternative, we used the steepest-descent method. It consists of three different steps: (1) find the minima, (2) find the first-order saddle points, and (3) find the steepest-descent trajectories from the saddle points to the connecting minima The whole method is highly deterministic and hence avoids the problems associated with the dragging method.

We used Baker's algorithm[36] to find the minima and the first-order saddle points. Baker uses the rational function optimization approach first described by Cerjan and Miller[37] to steer the search into the "correct" region of the configurational space. This approach requires information about both gradients and Hessians. A scheme for calculating gradients efficiently in generalized coordinates from Cartesian forces is described in the Appendix. Since the calculation and inversion of the Hessian can be computationally expensive, it is updated using a scheme by Powell[29] and only periodically recalculated. Initial configurations were generated by first placing the coadsorbed C_6 molecules in the intersections at the ends of either a straight or zigzag channel. The positions of the C_6 molecules were perturbed by short NVT Monte Carlo runs. Care was taken to ensure that the coadsorbed C_6 molecules did not leave the intersection by checking the distance moved by the coadsorbed molecule during the short Monte Carlo run. A methane molecule was then inserted within a radius of 10 Å around the coadsorbed molecules. 40 000 such initial configurations were generated for minima and saddle-point searches. Each search ended either when the norm of the gradient vector was less than a specified value or when the number of iterations exceeded an upper limit. We used a value of 5×10^{-5} kJ mol^{-1} Å^{-1} as the cutoff for the norm of the gradient and an upper limit of 1000 iterations. Baker's algorithm was able to find the appropriate stationary point for 95% of the initial configurations within the specified upper limit of the maximum iterations.

The steepest-descent path was found following the intrinsic reaction coordinate approach of Fukui[30] as used by Snurr et al.[35] (see note in the bibliography). As in the case of Snurr et al., we set the value of the distance moved to be 5×10^{-3} and then calculated a value of $d\tau$ using eqs 13 and 16 of ref 35, where τ is a scaling factor for how fast we move along the trajectory. The descent was terminated once the norm of the gradient was less than 5×10^{-4} kJ mol^{-1} Å^{-1}. Then the energy of the potential minimum was compared against a sorted list of the minima determined above. A successful match was found if the energy of a pretabulated minimum was within 5×10^{-3} kJ mol^{-1} of a minimum obtained from the steepest descent. Note that while it is not guaranteed to find the minima, a steepest-descent trajectory from a saddle point to a minimum that matches a pretabulated minimum is a strong check on the correctness of the code. While over 98% of the descents ended in pretabulated minima, some did not. This is not surprising since given the dimensionality of the system it is conceivable that our search for the minima was not exhaustive, and the descents actually find new minima.

MEP Results

Figure 3 shows a minimum energy path for methane in a straight channel diffusing past a benzene molecule in a channel intersection. The methane molecule starts in the center of the straight channel segment (point A). When the methane molecule is at point B, the benzene molecule moves into the energetically less favorable part of the intersection, increasing the total energy of the system but allowing the methane to move into the intersection. Going from point B to point C, the methane is moving into the zigzag channel, and benzene relaxes back to a more favorable part of the intersection. Finally, in the path shown, the methane molecule moves into the adjoining straight channel from point C to point D, again overcoming an energy barrier involving benzene movement in the intersection. The paths in the straight channels are symmetric about the center of the channel, consistent with the underlying symmetry of the

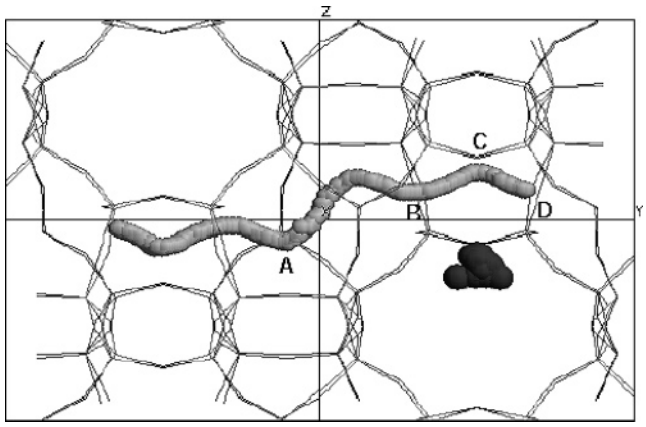

Figure 3. Minimum energy path for methane in a straight channel diffusing past a benzene molecule in a channel intersection. The center-of-mass positions of methane are shown in gray, and those of benzene are shown in black. Results shown were obtained with the dragging method.

zeolite straight channel. The zigzag channel paths (not shown), on the other hand, display no such symmetry, corroborating that the "zig" and the "zag" are structurally different. The position of cyclohexane is more localized for zigzag channel paths compared to straight channel paths. This suggests that depending on the direction of approach by the penetrant the blocking molecule has more or less freedom to move even though it is in the same site. Figure 4 shows the total potential energy of the system as a function of methane position for a key path in the zigzag channels. In both the straight and zigzag channels the activation energy with cyclohexane is much higher than that with benzene. This is expected since cyclohexane is a bulkier molecule and hence harder to pass than benzene.

The ranges of energies of minima and saddle-point searches are given in Table 1. A large number of paths have activation

TABLE 1: Ranges of Energies for the Minima and Saddle Points Searches for Cyclohexane and Benzene with Methane in the Two Different Channel Types

coadsorbed molecule	channel	minima (kJ/mol)		saddle points (kJ/mol)	
benzene	straight	−141.23	−123.66	−140.86	−79.87
benzene	zig-zag	−139.72	−127.44	−139.54	−95.11
cyclohexane	straight	−149.80	−125.79	−148.97	−100.23
cyclohexane	zig-zag	−148.22	−128.16	−148.21	−100.43

energies on the order of a few tenths of a kJ/mol, making them physically insignificant. A number of these low activation energy paths correspond to the small changes in the total energy due to blocking molecule rotations or slight reorientations. These changes are not of interest in calculating the paths taken by the methane to pass one of the C_6 molecules. To focus on the relevant paths, the steepest-descent calculation was only done for saddle points whose energies were at least 6 kJ/mol higher than the lowest minimum for that system. While this reduced the number of saddle points to descend from, it does not guarantee that we will not get low-activation energy paths. After doing the steepest-descent calculations for these paths, only those with activation energies greater than 6 kJ/mol were plotted (see Figures 5 and 6). These paths are in essence "projections" of the 15-dimensional path since we only see the methane motion in this figure. Using the definition of channels from Figure 1, we can describe three unique high-activation energy paths in Figures 5 and 6: methane going between a straight channel and the zig of a zigzag channel, between a straight channel and an intersection, and finally between an intersection and the zig. The minima within the straight and zigzag channels are connected by relatively low-activation energy paths which are not shown. This is physically reasonable since the benzene molecules are in the intersections, and only motion around them is likely to be activated.

Realizing that within each channel the methane equilibrates

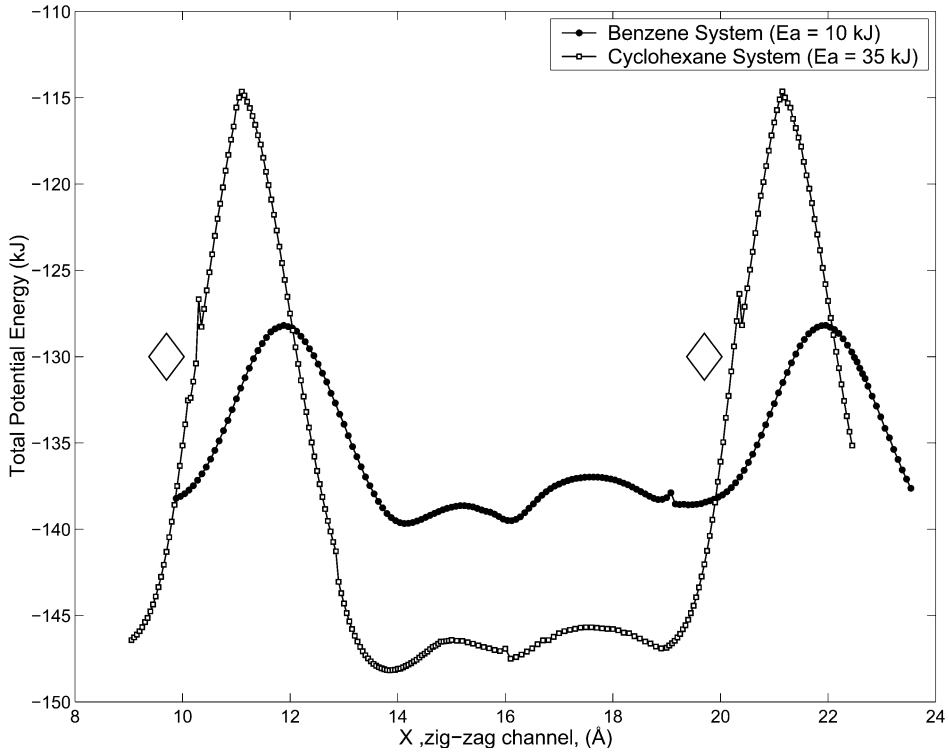

Figure 4. Activation energy of methane diffusion in zigzag channels with benzene and cyclohexane. The diamonds mark the approximate positions of the coadsorbed molecules in the intersections at the ends of the zigzag channel. Results shown were obtained with the dragging method, which causes small fluctuations in the energies.

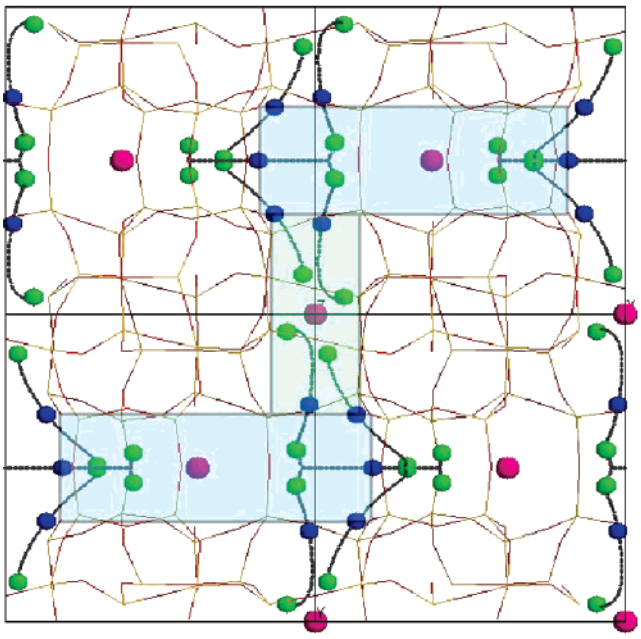

Figure 5. Selected minimum energy paths for the methane/benzene system. Only those paths with activation energy greater than 6 kJ/mol are shown. This is the same view as Figure 1. The green spheres mark the methane minima positions, and the blue spheres denote methane saddle point positions. The transparent blue rectangle marks the macrostate comprised of the zigzag channel and the intersection. The transparent green rectangle marks the macrostate in the straight channel. The red spheres are centers of each macrostate.

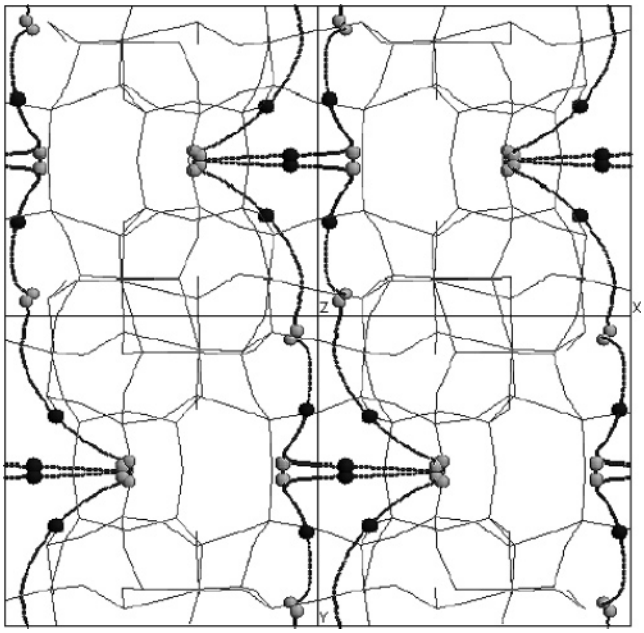

Figure 6. Selected minimum energy paths for the methane/cyclohexane system. Only those paths with activation energy greater than 6 kJ/mol are shown. The gray spheres represent methane minima positions, and the black spheres denote methane saddle point positions. The view is that of Figure 1.

rapidly, we can combine the minimum energy sites within each channel into a larger "macrostate". On the basis of the energies, we can identify two macrostates—one in the straight channel and the other comprised of the combined intersection and zigzag channel. These macrostates are shown by the transparent green and blue rectangles in Figure 5. Diffusion in the zeolite is then governed by hops between these macrostates, and with each hop the methane quickly equilibrates within the new macrostate.

TABLE 2: Activation Energies for Selected MEPs in the Methane/Benzene and Methane/Cyclohexane Systems

coadsorbate	state $i \rightarrow$ state j	ΔE_{ij} (kJ/mol)	ΔE_{ji} (kJ/mol)
benzene	I → S	13.1	15.4
cyclohexane	I → S	33.4	35.7
benzene	I → Z	10.3	11.4
cyclohexane	I → Z	32.5	33.3
benzene	S → Z	10.3	11.2
cyclohexane	S → Z	45.0	44.6

Each macrostate is assigned a center, indicated by a red sphere, calculated from the Boltzmann-weighted average positions of the minima comprising the macrostate. In the kinetic Monte Carlo simulations the lengths of hops between macrostates are calculated on the basis of the distance between the macrostate centers. The activation energies for each of the three paths are given in Table 2.

The MEPs are qualitatively the same for both systems, but the energies are much higher for cyclohexane as can be seen from Table 2. By comparing Figures 5 and 6, we see the MEPs for cyclohexane are slightly longer than those obtained for benzene. Interestingly, we found that the physical path of methane from the straight channel to the zigzag channel remained unchanged irrespective of the presence or absence of the cyclohexane in the intermediate intersection. However, the energy change was about 40 kJ/mol higher with the cyclohexane present in the intersection.

Free Energy Perturbation

The next step in calculating the diffusion coefficient of methane in silicalite when all intersections are occupied by benzene or cyclohexane is to obtain rate constants for each path shown in Figures 5 and 6. These rate constants will then be fed into a kinetic Monte Carlo (KMC) simulation to calculate the diffusivity.[4,32,38−40] Because of the high activation barriers, methane spends most of its time "rattling" in the relatively low potential regions of the sorption sites and only infrequently executing a diffusive hop over the high-energy barrier into a neighboring site. KMC focuses on these infrequent diffusive hopping events, enabling relatively large displacements to be simulated in a small amount of computer time compared to MD.

Theory

A number of methodologies have been used to calculate hopping rate constants from detailed atomistic models in zeolites.[35,41−44] Here we will use a thermodynamic perburation method described in detail by Theodorou.[45]

Consider a ν-dimensional system with low-lying sorption sites i and j connected by a minimum energy path and each consisting of a set of generalized coordinate positions $\{\mathbf{x}_i\}$, $\{\mathbf{x}_j\}$. Topologically, there will be at least one first-order saddle point $\mathbf{x}_{ij}^{S}$ between the two states. We can get an expression for the rate constant for hopping from i to j from transition-state theory (TST).[46,47] The TST rate constant can be expressed as a ratio of two configurational partition functions

$$k_{i\rightarrow j}^{\mathrm{TST}} = \frac{1}{\sqrt{2\beta\pi m^*}} \frac{\int_{S_{ij}} \mathrm{d}^{\nu-1} x \exp(-\beta \mathrm{V}(\mathbf{x}))}{\int_{\{i\}} \mathrm{d}^{\nu} x \exp(-\beta \mathrm{V}(\mathbf{x}))} \qquad (1)$$

where S_{ij} is a $(\nu - 1)$-dimensional dividing surface partitioning the configuration space into distinct "reactant" and "product" states, β is $1/kT$ where k is Boltzmann's constant, V is the system potential energy, and m^* is an effective mass of the system which will be discussed below.[48,49] It should be noted that the

rate constant obtained from TST is an upper bound since it does not take into account barrier recrossings or multiple transitions which may affect the overall rate constant. These effects can be accounted for by calculating a dynamical correction factor as in the work of June et al.[41] The behavior at the dividing surface is crucial in determining the number of barrier recrossings or multiple transitions and hence the magnitude of the correction. Unfortunately, it is difficult to obtain the optimal dividing surface and sample from it for multidimensional systems, making it impractical to calculate the rate constant directly from eq 1. To ensure adequate statistical sampling and convergence, we use a free energy perturbation technique.[45]

Consider a minimum energy path connecting minimum $\mathbf{x}_{m_i}$ with minimum $\mathbf{x}_{m_j}$ and going through the saddle point $\mathbf{x}_{ij}^{S}$. We discretize this path by a number of closely spaced $(\nu - 1)$-dimensional planes S_1, S_2, ..., S_n lying normal to the minimum energy path such that S_1 passes through the minimum $\mathbf{x}_{m_i}$ and plane S_n passes through the highest point on the free energy path, $\mathbf{x}_{\text{fnrg}}$. Note, as we will see, it is not necessary to know $\mathbf{x}_{\text{fnrg}}$ ahead of time. We can write eq 1 as follows:[45]

$$k_{i\to j}^{\text{TST}} = \frac{1}{\sqrt{(2\beta\pi m^*)}} \frac{\int_{S_{ij}} \mathrm{d}^{\nu-1} x \exp[-\beta V(\mathbf{x})]}{\int_{\{i\}} \mathrm{d}^{\nu} x \exp[-\beta V(\mathbf{x})]}$$

$$= \frac{1}{\sqrt{(2\beta\pi m^*)}} \times \frac{\int_{S_1} \mathrm{d}^{\nu-1} x \exp[-\beta V(\mathbf{x})]}{\int_{\{i\}} \mathrm{d}^{\nu} x \exp[-\beta V(\mathbf{x})]} \frac{\int_{S_2} \mathrm{d}^{\nu-1} x \exp[-\beta V(\mathbf{x})]}{\int_{S_1} \mathrm{d}^{\nu-1} x \exp[-\beta V(\mathbf{x})]} \times \ldots \frac{\int_{S_m} \mathrm{d}^{\nu-1} x \exp[-\beta V(\mathbf{x})]}{\int_{S_{m-1}} \mathrm{d}^{\nu-1} x \exp[-\beta V(\mathbf{x})]} \times \ldots \frac{\int_{S_n} \mathrm{d}^{\nu-1} x \exp[-\beta V(\mathbf{x})]}{\int_{S_{n-1}} \mathrm{d}^{\nu-1} x \exp[-\beta V(\mathbf{x})]} \tag{2}$$

We can convert the $(\nu - 1)$-dimensional integral over S_1 into a ν-dimensional integral by integrating over a slice of thickness Δx_1 located around the energy minimum $\mathbf{x}_{m_i}$ and then dividing by the thickness of the slice. Denote this region by ΔS_1. Then we can rewrite eq 2 as

$$\sqrt{(2\beta\pi m^*)} k_{i\to j}^{\text{TST}} = \frac{1}{\Delta x_1} \frac{\int_{\Delta S_1} \mathrm{d}^{\nu} x \exp[-\beta V(\mathbf{x})]}{\int_{\{i\}} \mathrm{d}^{\nu} x \exp[-\beta V(\mathbf{x})]} \prod_{p=2}^{p=n} \frac{\int_{S_p} \mathrm{d}^{\nu-1} x \exp[-\beta V(\mathbf{x})]}{\int_{S_{p-1}} \mathrm{d}^{\nu-1} x \exp[-\beta V(\mathbf{x})]} \tag{3}$$

The ratio of the ν-dimensional integrals is the probability of visiting the region ΔS_1 by a system that samples state *i*. This can be calculated from a NVT Monte Carlo simulation of the system over region *i* and counting the number of times it visits the region ΔS_1.

To calculate the ratio of $(\nu - 1)$-dimensional integrals, we make the approximation that if the planes are close together then they are practically parallel. If the spacing between the planes S_{p-1} and S_p is $\delta\mathbf{x}$ along the transition path, then for each point $\mathbf{x}_{p-1}$ in the plane S_{p-1} there is a point $\mathbf{x}_{p-1} + \delta\mathbf{x}$ in the plane S_p. Using this, we can rewrite the ratio of the p and $p - 1$ integrals as

$$\frac{\int_{S_p} \mathrm{d}^{\nu-1} x \exp[-\beta V(\mathbf{x})]}{\int_{S_{p-1}} \mathrm{d}^{\nu-1} x \exp[-\beta V(\mathbf{x})]} = \frac{\int_{S_{p-1}} \mathrm{d}^{\nu-1} x \exp[-\beta V(\mathbf{x}+\delta\mathbf{x})]}{\int_{S_{p-1}} \mathrm{d}^{\nu-1} x \exp[-\beta V(\mathbf{x})]}$$

$$= \frac{\int_{S_{p-1}} \mathrm{d}^{\nu-1} x \exp[-\beta V(\mathbf{x})] \exp\{-\beta[V(\mathbf{x}+\delta\mathbf{x}) - V(\mathbf{x})]\}}{\int_{S_{p-1}} \mathrm{d}^{\nu-1} x \exp(-\beta V(\mathbf{x}))}$$

$$= \langle \exp\{-\beta[V(\mathbf{x}+\delta\mathbf{x}) - V(\mathbf{x})]\} \rangle_{NVT,S_{p-1}} \tag{4}$$

The ratio of the integrals can be computed as a canonical ensemble average over the plane S_{p-1}. We can also relate the ratios of the integrals to the free energy change by rewriting them as ratio of the partition functions Q_p and Q_{p-1} as

$$\frac{\int_{S_p} \mathrm{d}^{\nu-1} x \exp[-\beta V(\mathbf{x})]}{\int_{S_{p-1}} \mathrm{d}^{\nu-1} x \exp[-\beta V(\mathbf{x})]} = \frac{Q_p}{Q_{p-1}}$$

$$= \frac{\exp(-\beta A_p)}{\exp(-\beta A_{p-1})} = \exp(-\beta \Delta A_{p-1}) \tag{5}$$

where we used the equation $Q_p = \exp(-\beta A_p)$.

The final equation for the rate constant is then

$$k_{i\to j}^{\text{TST}} = \frac{1}{\sqrt{(2\beta\pi m)}} \frac{1}{\Delta x_1} (\text{prob of visiting strip } \Delta S_1) \prod_{p=1}^{p=n-1} \times \langle \exp\{-\beta[V(\mathbf{x}+\delta\mathbf{x}) - V(\mathbf{x})]\} \rangle_{NVT,S_p} \tag{6}$$

It should be noted from eq 4 that the planes must be chosen close enough together so that $\exp\{-\beta[V(\mathbf{x} + \delta\mathbf{x}) - V(\mathbf{x})]\}$ contributes statistically to the overall average.

Simulation Details

Our system consists of 15 degrees of freedom: 3 rotational and 3 translational degrees of freedom for each of the 2 blocking molecules placed on either side of the channel and the 3 translational degrees of freedom for the penetrant in the channel. It is convenient to break up the calculation of the rate constant $k_{i\to j}^{\text{TST}}$ into two parts. The first part involves the calculation of the ratios of the $(\nu - 1)$-dimensional integrals using the canonical ensemble sampling over the different planes. The second part is the calculation of the probability of visiting the initial strip ΔS_1.

To focus on the rare event transitions between states, we selected those MEPs with activation energies greater than $2.5kT$. Since all simulations were done at 300 K, all paths with activation energies less than about 6 kJ/mol were discarded. States connected with lower activation energies paths were assumed to be in equilibrium with each other. Images of the paths were then generated over the entire silicalite unit cell using symmetry operators consistent with the *Pnma* symmetry of ORTHO silicalite. The MEP path was broken into a number points such that the greatest center-of-mass distance moved by a molecule between two points was ≤ 0.1 Å. The normal $\mathbf{n}_p$ at

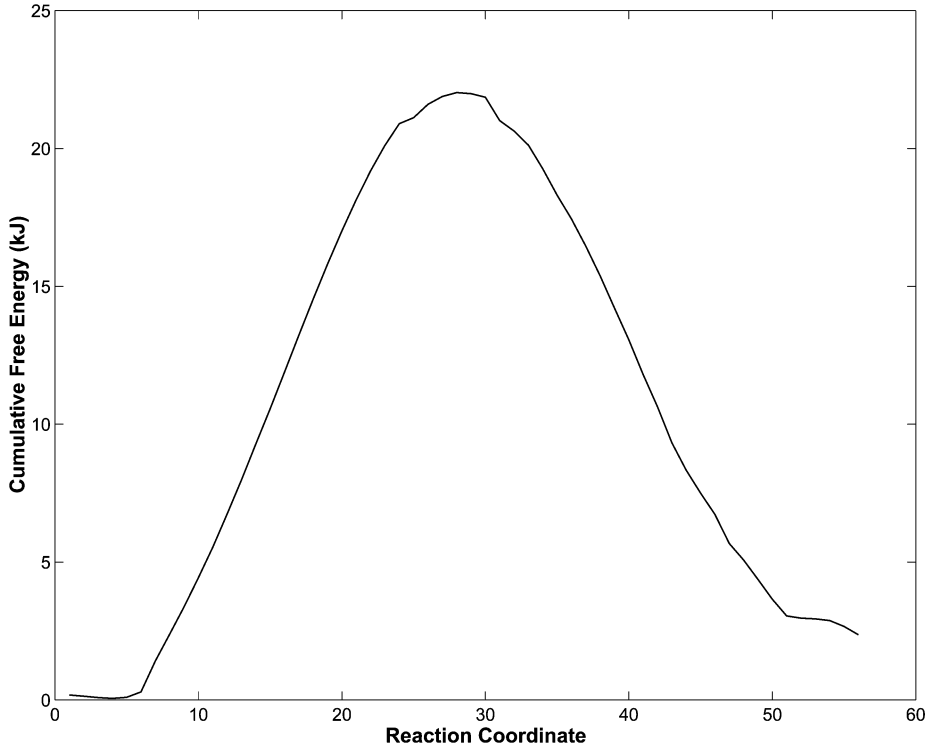

Figure 7. Free energy plot of methane/benzene system. The MEP is going from an intersection to a zig site. The abscissa is the plane number along this MEP.

the point $\mathbf{x}_p$ was approximated by the secant vector between the points $\mathbf{x}_p$ and $\mathbf{x}_{p-1}$ on the MEP.

Monte Carlo simulations in the NVT ensemble were used to calculate the change in free energy between each plane and the next one. Monte Carlo moves constrained to the 14-dimensional hyperplane of interest were done by displacing the system in 15-dimensions and then projecting the displacement vector on to the hyperplane using the following algorithm[50]

$$\Delta\mathbf{x}_{\text{disp}} = \mathbf{x}_{\text{r}} - \mathbf{x}_{\text{p}}$$
$$\mathbf{x}_{\text{new}} = \Delta\mathbf{x}_{\text{disp}} - \Delta\mathbf{x}_{\text{disp}}\cdot\mathbf{n}_{\text{p}} + \mathbf{x}_{\text{p}} \quad (7)$$

where $\mathbf{x}_{\text{r}}$ are the coordinates of the system after the random displacement and $\mathbf{x}_{\text{new}}$ is the displaced point in the constraint plane. 300 000−600 000 iterations were done in each plane to calculate the change in free energy. As a check on the convergence, the perturbation simulations were done in both directions along a MEP and the results compared. The results were independent of the direction as expected.

The second part of the rate constant involves the calculation of the probability of being in the vicinity of the minimum energy site. If we denote the first point on the MEP as $\mathbf{x}_1$ and the normal at $\mathbf{x}_1$ as $\mathbf{n}_1$ and two points $\mathbf{x}_{q1}$ and $\mathbf{x}_{q2}$ such that

$$\mathbf{x}_{q1} = \mathbf{x}_1 + (\mathbf{n}_1\Delta x_1/2)$$
$$\mathbf{x}_{q2} = \mathbf{x}_1 - (\mathbf{n}_1\Delta x_1/2) \quad (8)$$

where Δx_1 is the thickness of the strip, we can then generate two 14-dimensional planes as boundaries of the "slice" in which we need to calculate the visiting probability. The equations of these planes are given by

$$\text{plane 1:} \quad (\mathbf{x} - \mathbf{x}_{q1})\cdot\mathbf{n}_1 = 0$$
$$\text{plane 2:} \quad (\mathbf{x} - \mathbf{x}_{q2})\cdot\mathbf{n}_1 = 0 \quad (9)$$

A slice thickness of 0.5 Å was taken for all of the probability calculations.

The final part of the rate calculation requires the "mass" of the hopping system. If the transition involves the concerted movement of a number of degrees of freedom, then the mass associated with the transition can be difficult to calculate. Vineyard[48] calculates the effective mass based on a weighted average of the mass associated with the motion along each degree of freedom across the saddle point. An estimate of the motion along each degree of freedom can be obtained from the eigenvector corresponding to the negative eigenvalue at the saddle point. In our simulations, visualizations of the MEPs show that the transition across the saddle point is dominated by the motion of methane, making it a good approximation to set the effective mass to the mass of methane.

Results

Figure 7 shows the free energy profile for one of the three unique paths shown in Figure 5. The free energy of the first minimum is used as a reference in each case, and the free energy difference is accumulated for each plane until reaching the second minimum. The abscissa is the number of the plane along the minimum energy path and can be considered as an arbitrary reaction coordinate. For the Monte Carlo calculation in each plane the ratio of the configuration integrals was plotted to ensure convergence (not shown). The standard deviation of the ratio of configuration integrals over the run length was on the order of 10^{-2} kJ/mol for each plane, and on an average there are about 50−70 planes for each path, giving an overall uncertainty of about 0.5 kJ/mol. The free energies of activation for each path, the probability of visiting the initial slice, and the final TST rate constants are given in Table 3. By contrasting the activation free energies with the activation energies of the MEPs from Table 2, we see that entropy plays an important role in the determination of the free energies.

Using the rate constants from Table 3 and the definitions of the macrostates, we calculated the diffusivity of methane in the presence of benzene from a KMC simulation as described

TABLE 3: Probability of Visiting a Narrow Strip around State *i*, the Free Energy of Activation between States *i* and *j*, and the Overall TST Rate Constant for the Methane/Benzene System[a]

state $i \rightarrow$ state j	prob(i)	ΔA_{ij} (kJ/mol)	k_{ij}^{TST} (s^{-1})
I → S	0.120	14.5	3.577×10^7
S → I	0.120	11.8	1.057×10^8
I → Z	0.120	22.0	1.768×10^6
Z → I	0.063	19.6	2.430×10^6
S → Z	0.024	6.5	1.765×10^8
Z → S	0.019	9.7	3.874×10^7

[a] The symbols I, S, and Z correspond to intersection, straight channel, and zig of the zig-zag channel, respectively.

elsewhere.[35,38,41] The loading of benzene was taken to be 4 molecules/unit cell adsorbed at the 4 unit cell intersections. During the free energy calculation the benzene stays in the intersection, suggesting that the activation energy for the benzene hopping is higher than that for methane. This is supported by comparing the rate constants in Table 3 to those for pure benzene given in the work of Snurr et al.[35] which used the same potential model for the system. We find that the methane motion occurs 3−4 orders of magnitude faster than the hopping motion of benzene. In addition, the overall activation energy reported by Snurr et al. is 36 kJ/mol, which is considerably higher than the activation energies reported in Table 2. Consequently, it is reasonable to assume that the benzene is fixed at the intersections during the time scales spanned by the motion of methane.

We used 500 methane "ghost" molecules in the KMC simulation, initially distributed randomly over the eight macrostates. After a few thousand iterations an equilibrium probability distribution that is consistent with the transition rates is attained. The mean-squared displacement of methane averaged over the 500 systems is plotted in Figure 8. The lines are linear as expected, and the self-diffusivity can be obtained from the slopes of the lines using the Einstein equation. It should be noted that the diffusivity in the zigzag channels (*x*-direction) is greater than that in the straight channels (*y*-direction). This is interesting since the zigzag channels have a greater tortuosity than the straight channels, making single-component diffusion for both methane[51] and benzene[35] higher in the straight channels. The diffusivity of methane with varying loadings of benzene is given in Table 4. The diffusivity of methane drops by over an order of magnitude in going from 3 to 4 molecules/unit cell of benzene. The value at 4 benzene per unit cell is too small to be obtained by a conventional molecular dynamics simulation.

TABLE 4: Diffusivity of Methane at Various Loadings of Coadsorbed Benzene[a]

methane loading (molecules/uc)	benzene loading (molecules/uc)	methane diffusivity (m^2/s)
3	0	1.29×10^{-8}
3	1	4.82×10^{-9}
3	2	9.71×10^{-10}
3	3	3.54×10^{-10}
1	4	2.51×10^{-11}

[a] The first four points were generated using molecular dynamics simulations, and the fifth point was generated using kinetic Monte Carlo.

Figure 9 shows the scatter plot of methane and cyclohexane in a plane along a MEP going from an intersection to a straight channel. The arrow in the figure indicates the hopping motion of cyclohexane from the intersection to the adjacent straight channel as the methane gets close to it. This suggests that methane can only get through to the other channels by actually displacing the cyclohexane in the intersection. The activation energy of cyclohexane diffusion as observed experimentally[52] is approximately 48 kJ/mol. This value is close to the activation energies observed in Table 2, further suggesting that the actual mode of methane passage may involve a concerted cyclohexane hop. The motion of cyclohexane drastically increases the number

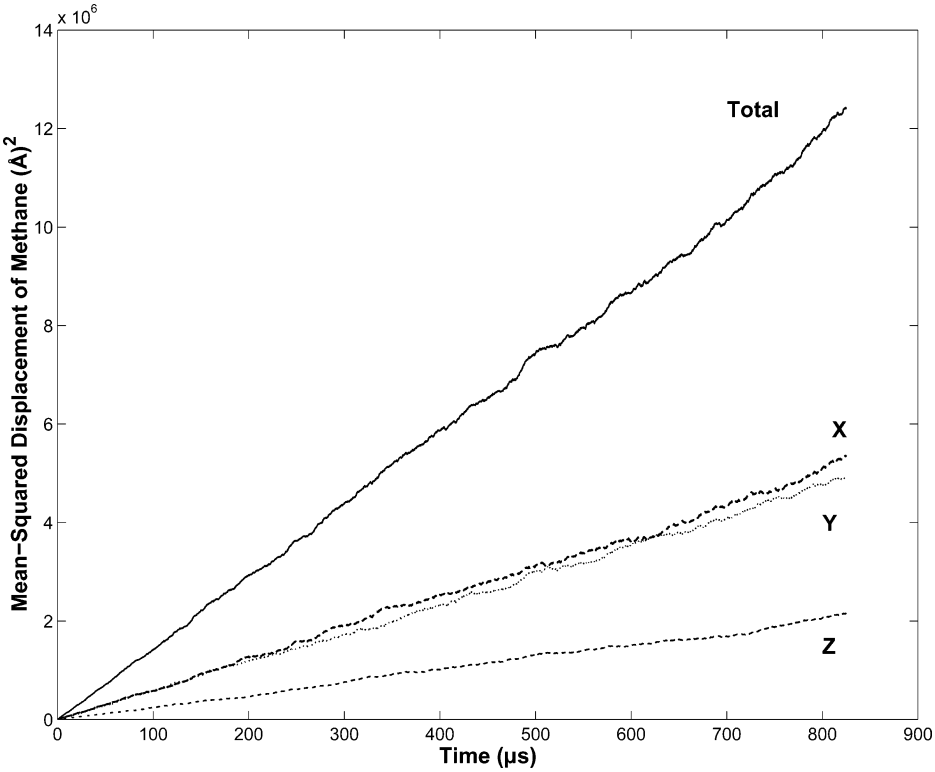

Figure 8. Mean-squared displacements of methane coadsorbed with 4 benzene per unit cell. Kinetic Monte Carlo allows simulations even at microsecond time scales. The mean-squared displacement in the *x*-direction is slightly higher than the *y*-direction as discussed in the text.

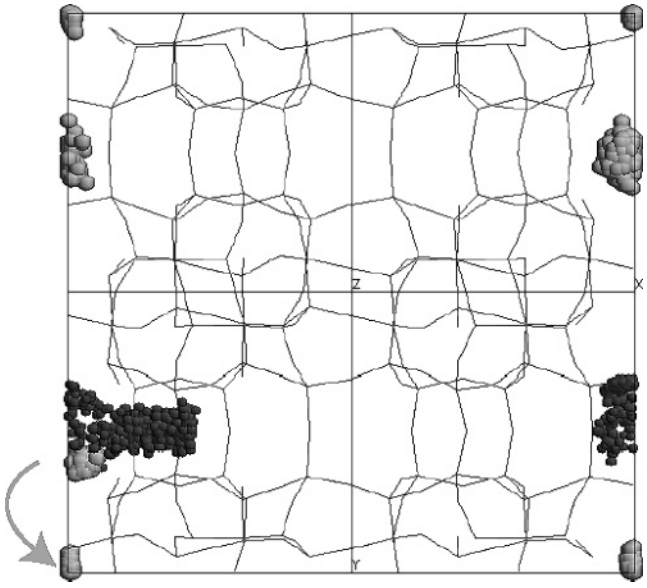

Figure 9. Scatter plot of methane with cyclohexane from a Monte Carlo simulation where the system is confined to a 14-dimensional hyperplane along the straight-to-intersection MEP. The gray spheres are the centers-of-mass of cyclohexane whereas the black spheres denote the centers-of-mass of methane molecules. The arrow shows the hopping motion of cyclohexane from the intersection to the straight channel.

of possible macrostates and the rate constants that need to be computed, making this approach impractical for this system. It should be possible to develop and implement alternative methodologies such as accelerated molecular dynamics[53,54] to treat such problems in the future.

With systems that are so confined it is reasonable to expect the flexibility of the zeolite lattice to play a significant role in determining the overall diffusion kinetics. This was demonstrated recently by Forester and Smith[55] for benzene in silicalite. Lattice flexibility could be incorporated into our approach in the free energy calculations, for example, by using hybrid Monte Carlo[56,57] or perhaps more directly in an accelerated MD treatment of diffusion.

Conclusions

In this work we have used and extended computational methodologies to gain insight into the mechanisms of pore blockage in microporous media. First, molecular dynamics simulations were used to examine the effects of degree of pore blockage for methane in silicalite by varying the loading of larger coadsorbed molecules. We observed a decrease in the diffusivity of the penetrant as the loading of coadsorbed molecules was increased from 1 to 4 molecules/unit cell. The decrease was particularly great in going from 3 to 4 molecules/unit cell for the cases of benzene and cyclohexane. This decrease can be explained on the basis of the siting of the penetrant and the coadsorbed molecule. The bulkier coadsorbed molecules, benzene and cyclohexane, prefer to adsorb in the channel intersections, whereas methane prefers the channels where it can interact strongly with the pore walls. At coadsorbate loadings of 4 molecule/unit cell the benzene and cyclohexane molecules effectively trap the methane molecules in the channels on MD time scales.

Because molecular dynamic simulations are too inefficient to sample the rare-event crossings of methane past the coadsorbed molecules, it is difficult to obtain the diffusivities of the penetrant directly from MD. Calculating minimum energy paths provides a viable approach to gain fundamental mechanistic insight into the dynamics of the penetrant/coadsorbate/zeolite system and to get activation energies for the crossing rates. This is the first step toward getting rate constants which can then be used in a kinetic Monte Carlo simulation to get the diffusivities. Two different approaches were compared for getting the minimum energy paths. While it is easier to implement the dragging method to get the minima in each plane, it is difficult to ensure that the paths obtained are physically meaningful. The steepest-descent method, on the other hand, provided us with physically meaningful minimum energy paths. The activation energies for methane passing cyclohexane were found to be larger than those for passing benzene.

On the basis of the activation energies of the minimum energy paths obtained for methane with coadsorbed benzene in silicalite, we divided the zeolite unit cell into eight macrostates each of which consists of a number of minima or microstates. Within each macrostate the minima were connected by paths of relatively low activation energies, and we assumed that once the system enters a macrostate it can equilibrate rapidly with the minima lying inside that macrostate. Using the free energy perturbation scheme, free energies of activation were obtained along different minimum energy paths connecting the various macrostates. Comparing the activation energies obtained from the free energy calculation and activation energies reported for the diffusion of pure benzene, it seemed reasonable to assume that benzene is fixed in the silicalite intersections on methane diffusion time scales. With this assumption and using the rate constants obtained from the free energy calculation, kinetic Monte Carlo simulations were used to calculate the diffusivity of methane in the presence of 4 benzene molecules per unit cell. The mean-squared displacements are highest in the *x*-direction (zigzag channels), contrary to the observance in single-component systems in silicalite where mean-square displacement is highest in the *y*-direction (straight channels).

Free energy perturbation calculations were also used for methane in the presence of cyclohexane. This system shows different behavior from that of benzene, in that cyclohexane hops out of the intersection and into the straight channel when approached by a methane molecule. This suggests that a mechanism for the passage of methane probably involves a concerted hop by the cyclohexane and methane. The hopping mechanism drastically increases the number of macrostates and hence the number of possible transitions making the rate calculation and kinetic Monte Carlo simulations impractical.

Acknowledgment. This work has been supported by the National Science Foundation.

Appendix. Calculating Derivatives in Generalized Coordinates

Minimizing an objective function with respect to Cartesian atomic positions can be difficult for rigid molecules due to the presence of intramolecular geometric constraints. It is often more convenient to work in a coordinate system where the constraints can be included more naturally and do not play a direct role in the minimization. For instance, a rigid polyatomic molecule having 6 degrees of freedom can be fully specified by its 3 center-of-mass coordinates and 3 Eulerian angles[58] given the relative coordinates of the atoms within the molecule in an arbitrary coordinate system.

Let the Cartesian coordinates in the zeolite for methane and the atoms of two blocking molecules be defined by the position vectors $\mathbf{r}^{m}$, $\mathbf{r}_i^{b1}$, and $\mathbf{r}_j^{b2}$, respectively, where methane is defined as a single sphere, $1 \leq i, j \leq 6$ for cyclohexane, and $1 \leq i, j \leq$

12 for benzene. The components of the vectors are denoted by x^m, y^m, z^m, x_i^{b1}, y_i^{b1}, ... Then the objective function V is given by

$$V(\mathbf{r}^m,\mathbf{r}_i^{b1},\mathbf{r}_j^{b2}) = V_m(\mathbf{r}^m) + V_{b1}(\mathbf{r}_i^{b1}) + V_{b2}(\mathbf{r}_j^{b2}) + V_{mb1}(\mathbf{r}^m,\mathbf{r}_i^{b1}) + V_{mb2}(\mathbf{r}^m,\mathbf{r}_j^{b2}) + V_{b1b2}(\mathbf{r}_i^{b1},\mathbf{r}_j^{b2}) \quad (10)$$

where the first three terms on the right-hand side indicate sorbate−zeolite interactions and the rest of the terms indicate sorbate−sorbate interactions. Each term is calculated by summing the Lennard-Jones plus electrostatic interactions between all pairs of "atoms" in the zeolite/molecule system.

To carry out the minimization in the new coordinate system, the generalized coordinates, we need to calculate the gradient of the objective function V with respect to the new variables. Let us define a body coordinate system with its axes along the principal axes of the moment of inertia of the molecule and its origin at the center-of-mass of the molecule. Let the position vector, in the local body coordinate system, of the atom i in blocking molecule 1 be denoted by $\mathbf{r}_{ibody}^{b1}$. Then if we denote the position vector of the center-of-mass coordinates of one blocking molecule by $\mathbf{r}_{com}^{b1}$ with components (x_{com}^{b1}, y_{com}^{b1}, z_{com}^{b1}) and the Eulerian angles by (θ^{b1}, ϕ^{b1}, ψ^{b1}), we can write the Cartesian coordinates for each atom i of the blocking molecule in terms of the generalized coordinates using the following equation:

$$\mathbf{r}_i^{b1} = \mathbf{r}_{com}^{b1} + \mathbf{T}(\theta^{b1}, \phi^{b1}, \psi^{b1})\cdot\mathbf{r}_{ibody}^{b1} \quad (11)$$

Here $\mathbf{T}$ is a transformation matrix that takes coordinates from a local coordinate system to a fixed coordinate system.[58] Then the problem boils down to finding the derivatives of V with respect to each of the generalized coordinates using eqs 10 and 11. Although this is a simple if rather tedious application of the chain rule to each term of eq 10, we can simplify the process by calculating the gradients in Cartesian coordinates and transforming them as illustrated below.

We will calculate the gradient of V with respect to the generalized coordinates of blocking molecule 1 (x_{com}^{b1}, y_{com}^{b1}, z_{com}^{b1}, θ^{b1}, ϕ^{b1}, ψ^{b1}). First, we demonstrate this for the center-of-mass coordinates. Differentiating V with respect to x_{com}^{b1} and applying the chain rule, we get the following expression if the blocking molecule b1 is benzene ($1 \le i \le 12$):

$$\frac{\partial V}{\partial x_{com}^{b1}} = \sum_{i=1}^{12} \frac{\partial V}{\partial x_i^{b1}}\frac{\partial x_i^{b1}}{\partial x_{com}^{b1}} + \sum_{i=1}^{12} \frac{\partial V}{\partial y_i^{b1}}\frac{\partial y_i^{b1}}{\partial x_{com}^{b1}} + \sum_{i=1}^{12} \frac{\partial V}{\partial z_i^{b1}}\frac{\partial z_i^{b1}}{\partial z_{com}^{b1}} \quad (12)$$

Since each term in eq 10 is of the Lennard-Jones or the Coulombic potential form, it is relatively straightforward to calculate the gradient of V with respect to the Cartesian atom coordinates.[24] Let us denote these gradients by g_{xi}^{b1}, g_{yi}^{b1}, and g_{zi}^{b1} for $\partial V/\partial x_i^{b1}$, $\partial V/\partial y_i^{b1}$, and $\partial V/\partial z_i^{b1}$, respectively. To get the derivatives of the Cartesian coordinates with respect to the generalized coordinates, it is helpful to rewrite eq 11 in terms of its components.

$$x_i^{b1} = x_{com}^{b1} + (T_{11}, T_{12}, T_{13})\cdot\mathbf{r}_{ibody}^{b1}$$

$$y_i^{b1} = y_{com}^{b1} + (T_{21}, T_{22}, T_{23})\cdot\mathbf{r}_{ibody}^{b1}$$

$$z_i^{b1} = z_{com}^{b1} + (T_{31}, T_{32}, T_{33})\cdot\mathbf{r}_{ibody}^{b1} \quad (13)$$

From eq 13 it is easy to see that $\partial x_i^{b1}/\partial x_{com}^{b1} = 1$ and $\partial y_i^{b1}/\partial x_{com}^{b1}$, $\partial z_i^{b1}/\partial x_{com}^{b1} = 0$. Therefore, eq 12 now becomes

$$\frac{\partial V}{\partial x_{com}^{b1}} = \sum_{i=1}^{12} g_{xi}^{b1} \quad (14)$$

By symmetry, we can see that the gradient of V with respect to a center-of-mass coordinate is simply the sum of the gradients on all the atoms in that direction.

Now to calculate the gradient with respect to θ or the other Eulerian angles we need

$$\frac{\partial V}{\partial \theta^{b1}} = \sum_{i=1}^{12} \frac{\partial V}{\partial x_i^{b1}}\frac{\partial x_i^{b1}}{\partial \theta^{b1}} + \sum_{i=1}^{12} \frac{\partial V}{\partial y_i^{b1}}\frac{\partial y_i^{b1}}{\partial \theta^{b1}} + \sum_{i=1}^{12} \frac{\partial V}{\partial z_i^{b1}}\frac{\partial z_i^{b1}}{\partial \theta^{b1}} \quad (15)$$

Substituting for the Cartesian gradients and taking the derivative with respect to θ^{b1} on both sides of eq 13, we get

$$\frac{\partial V}{\partial \theta^{b1}} = \sum_{i=1}^{12}\left[g_{xi}^{b1}\frac{\partial(T_{11},T_{12},T_{13})}{\partial \theta^{b1}}\cdot\mathbf{r}_{ibody}^{b1} + g_{yi}^{b1}\frac{\partial(T_{21},T_{22},T_{23})}{\partial \theta^{b1}}\cdot\mathbf{r}_{ibody}^{b1} + g_{zi}^{b1}\frac{\partial(T_{31},T_{32},T_{33})}{\partial \theta^{b1}}\cdot\mathbf{r}_{ibody}^{b1}\right] \quad (16)$$

This can be rewritten using matrix notation as

$$\frac{\partial V}{\partial \theta^{b1}} = \sum_{i=1}^{12}(g_{xi}^{b1}, g_{yi}^{b1}, g_{zi}^{b1})\cdot\frac{\partial \mathbf{T}}{\partial \theta}\cdot\mathbf{r}_{ibody}^{b1} \quad (17)$$

We can obtain similar expressions for the other two Eulerian angles. Hence, by multiplying the Cartesian forces by the derivative of our transformation matrix times the body coordinates, we can generate the gradients in the generalized coordinates.

References and Notes

(1) Kärger, J.; Ruthven, D. M. *Diffusion in Zeolites*; Wiley: New York, 1992.

(2) Theodorou, D. N.; Snurr, R. Q.; Bell, A. T. In *Comprehensive Supramolecular Chemistry*; Alberti, G., Bein, T., Eds.; Pergamon: Oxford, 1996; pp 507−548.

(3) Auerbach, S. M. *Int. Rev. Phys. Chem.* **2000**, *19*, 155−198.

(4) Keil, F. J.; Krishna, R.; Coppens, M. O. *Rev. Chem. Eng.* **2000**, *16*, 71−197.

(5) Skoulidas, A. I.; Sholl, D. S. *J. Phys. Chem. A* **2003**, *107*, 10132−10141.

(6) Maginn, E. J.; Bell, A. T.; Theodorou, D. N. *J. Phys. Chem.* **1993**, *97*, 4173−4181.

(7) Snurr, R. Q.; Kärger, J. *J. Phys. Chem. B* **1997**, *101*, 6469−6473.

(8) Gergidis, L. N.; Theodorou, D. N. *J. Phys. Chem. B* **1999**, *103*, 3380−3390.

(9) Sanborn, M. J.; Snurr, R. Q. *Sep. Purif. Technol.* **2000**, *20*, 1−13.

(10) Sanborn, M. J.; Snurr, R. Q. *AIChE J.* **2001**, *47*, 2032−2041.

(11) Kamala, C. R.; Ayappa, K. G.; Yashonath, S. *Phys. Rev. E* **2002**, *65*, 061202.

(12) Skoulidas, A. I.; Sholl, D. S.; Krishna, R. *Langmuir* **2003**, *19*, 7977−7988.

(13) Theodorou, D.; Wei, J. *J. Catal.* **1983**, *83*, 205−224.

(14) Förste, C.; Germanus, A.; Kärger, J.; Pfeifer, H.; Caro, J.; Pilz, W.; Zikánová, A. *J. Chem. Soc., Faraday Trans. 1* **1987**, *83*, 2301−2309.

(15) Nelson, P. H.; Bibby, D. M.; Kaiser, A. B. *Zeolites* **1991**, *11*, 337−344.

(16) van Koningsveld, H.; Tuinstra, F.; van Bekkum, H.; Jansen, J. C. *Acta Crystallogr.* **1989**, *B45*, 423−431.

(17) Kiselev, A. V.; Lopatkin, A. A.; Shulga, A. A. *Zeolites* **1985**, *5*, 261−267.
(18) Snurr, R. Q.; Bell, A. T.; Theodorou, D. N. *J. Phys. Chem.* **1993**, *97*, 13742−13752.
(19) Goodbody, S. J.; Watanabe, K.; MacGowan, D.; Walton, J. P. R. B.; Quirke, N. *J. Chem. Soc., Faraday Trans.* **1991**, *87*, 1951−1958.
(20) June, R. L.; Bell, A. T.; Theodorou, D. N. *J. Phys. Chem.* **1992**, *96*, 1051−1060.
(21) Rowley, R. L.; Ely, J. F. *Mol. Phys.* **1992**, *75*, 713−730.
(22) Gupta, A.; Clark, L. A.; Snurr, R. Q. *Langmuir* **2000**, *16*, 3910−3919.
(23) Edberg, R.; Evans, D. J.; Morriss, G. P. *J. Chem. Phys.* **1986**, *84*, 6933−6939.
(24) Allen, M. P.; Tildesley, D. J. *Computer Simulation of Liquids;* Oxford University Press: New York, 1987.
(25) Ciccotti, G.; Ferrario, M.; Ryckaert, J.-P. *Mol. Phys.* **1982**, *47*, 1253−1264.
(26) Gupta, A. Computer Simulation of Multi-Component Adsorption and Diffusion in Silicalite Zeolite. Ph.D. Thesis, Northwestern University, 2000.
(27) Schuring, D.; Koriabkina, A. O.; de Jong, A. M.; Smit, B.; van Santen, R. A. *J. Phys. Chem. B* **2001**, *105*, 7690−7698.
(28) Sevick, E. M.; Bell, A. T.; Theodorou, D. N. *J. Chem. Phys.* **1993**, *98*, 3196−3212.
(29) Press, W. H.; Teukolsky, S. A.; Vellerling, W. T.; Flannery, B. P. *Numerical Recipes in C*, 2nd ed.; Cambridge University Press: New York, 1993.
(30) Fukui, K. *Acc. Chem. Res.* **1981**, *14*, 363−368.
(31) Bell, S.; Crighton, J. S. *J. Chem. Phys.* **1984**, *80*, 2464−2475.
(32) Auerbach, S. M.; Henson, N. J.; Cheetham, A. K.; Metiu, H. I. *J. Phys. Chem.* **1995**, *99*, 10600−10608.
(33) Jónsson, H.; Mills, G.; Jacobsen, K. W. In *Classical and Quantum Dynamics in Condensed Phase Simulations*; Berne, B. J., Ciccotti, G., Coker, D. F., Eds.; World Scientific: River Edge, NJ, 1998; Chapter 16.
(34) Bolhuis, P. G.; Dellago, C.; Geissler, P. L.; Chandler, D. *J. Chem. Phys.* **1998**, *108*, 9236−9245.
(35) Snurr, R. Q.; Bell, A. T.; Theodorou, D. N. *J. Phys. Chem.* **1994**, *98*, 11948−11961. Erratta: Although the correct equations were used in the actual calculations, there is an error in the paper: The fourth equation in the set of equations marked (12) on p 11951 should read: $(I_1 \sin^2\theta \sin^2\psi + I_2 \sin^2\theta \cos^2\psi + I_3 \cos^2\theta)\,d\varphi + (I_1 \sin\theta \sin\psi \cos\psi - I_2 \sin\theta \cos\psi \sin\psi)\,d\theta + (I_3 \cos\theta)\,d\psi = -(\partial V/\partial\phi)t\,dt$.
(36) Baker, J. *J. Comput. Chem.* **1986**, *7*, 385−395.
(37) Cerjan, C. J.; Miller, W. H. *J. Chem. Phys.* **1981**, *75*, 2800−2806.
(38) Tsikoyiannis, J. G.; Wei, J. *Chem. Eng. Sci.* **1991**, *46*, 233−253.
(39) Auerbach, S. M.; Bull, L. M.; Henson, N. J.; Metiu, H. I.; Cheetham, A. K. *J. Phys. Chem.* **1996**, *100*, 5923−5930.
(40) Saravanan, C.; Auerbach, S. M. *J. Chem. Phys.* **1999**, *110*, 11000−11011.
(41) June, R. L.; Bell, A. T.; Theodorou, D. N. *J. Phys. Chem.* **1991**, *95*, 8865−8878.
(42) Sholl, D. S. *Chem. Eng. J.* **1999**, *74*, 25−32.
(43) Dubbeldam, D.; Calero, S.; Maesen, T. L. M.; Smit, B. *Phys. Rev. Lett.* **2003**, *90*, 245901.
(44) Turaga, S. C.; Auerbach, S. M. *J. Chem. Phys.* **2003**, *118*, 6512−6517.
(45) Theodorou, D. N. In *Diffusion in Polymers*; Neogi, P., Ed.; Marcel Dekker: New York, 1996; Chapter 2, pp 67−142.
(46) Gladstone, S.; Laidler, K. J.; Eyring, H. *The Theory of Rate Processes*, 1st ed.; McGraw-Hill Book Co.: New York, 1941.
(47) Hill, T. L. *An Introduction to Statistical Thermodynamics;* Addison-Wesley: Reading, MA, 1962; reprint published by Dover Publications: Mineola, NY, 1986.
(48) Vineyard, G. H. *J. Phys. Chem. Solids* **1957**, *3*, 121−127.
(49) Greenfield, M. L.; Theodorou, D. N. *Macromolecules* **1998**, *31*, 7068−7090.
(50) The equations presented here are only applicable for an orthogonal coordinate system, and in general the coordinate system parametrized by the generalized coordinates is not orthogonal. This is only a concern in the calculation of forces and following system dynamics since in that case each generalized coordinate has a role in defining the metric of the space which governs the motion of the system. However, for purposes of calculating energy, we can consider the energy as a mathematical function of 15 variables which are components of an orthogonal basis without it affecting the value of the energy. Hence, for our purpose we consider the generalized coordinates just as a set of 15 number defining a vector in 15-dimensional rectangular space.
(51) June, R. L.; Bell, A. T.; Theodorou, D. N. *J. Phys. Chem.* **1990**, *94*, 8232−8240.
(52) Magalhães, F. D.; Laurence, R. L.; Conner, W. C. *J. Phys. Chem. B* **1998**, *102*, 2317−2324.
(53) Voter, A. F. *J. Chem. Phys.* **1997**, *106*, 4665−4677.
(54) Sørenson, M. R.; Voter, A. F. *J. Chem. Phys.* **2000**, *112*, 9599−9607.
(55) Forester, T. R.; Smith, W. *J. Chem. Soc., Faraday Trans.* **1997**, *93*, 3249−3257.
(56) Duane, S.; Kennedy, A. D.; Pendleton, B. J.; Roweth, D. *Phys. Lett. B* **1987**, *195*, 216−222.
(57) Brotz, F. A.; Pablo, J. J. D. *Chem. Eng. Sci.* **1994**, *49*, 3015−3031.
(58) Marion, J. B.; Thornton, S. T. *Classical Dynamics of Particles and Systems*, 4th ed.; Saunders College Publishing: Philadelphia, PA, 1995.